MODULATION TRANSFER FUNCTION COMPENSATION FOR OPTICAL SATELLITE IMAGE RESTORATION USING JOINT STATISTICAL MODEL IN CURVELET DOMAIN

Soo Mee Jessica Wong, Su Wai Ng, Adhwa Amir Tan

National Space Agency, Ministry of Energy, Science, Technology, Environment and Climate Change, 42700 Banting, Malaysia
Email: jessica@angkasa.gov.my; wayne@angkasa.gov.my; adhwa@angkasa.gov.my

KEY WORDS: Regularization-terms, image prior, image fidelity, nonlocal self-similarity, Bilevel optimization

Abstract. The heavy-tailed properties of Modulation Transfer Function (MTF) typically introduces noise and an unacceptable aliasing effect in the MTF compensation (MTFC) effort for spatial image quality improvement. These degradative effects compromise the image's Signal to Noise (SNR). Consequently, users must evaluate the relative importance of image sharpness versus noise to their applications in deciding whether MTFC processing is appropriate. In this paper, we present a strategy for high-fidelity MTF compensation framework by characterizing the local smooth and nonlocal self-similarity properties of optical satellite images in hybrid space and frequency domain. To realize the objective of this work, we design regularization terms that reflect the local smoothness and nonlocal self-similarity properties of the image and establish a simple joint statistical model in Curvelet domain to combine these two properties. To make the regularization-based MTFC method tractable and robust, we employ multi-objective bilevel optimization approach to efficiently solve the severely ill-posed inverse problem of MTFC. We conduct extensive experiments to evaluate the proposed regularization-based MTFC method using synthetically blurred images simulated from level 2A product of IKONOS. Quantitative measurements of image quality reveal that the proposed method produces competitive restoration results with minimum computational complexity and exhibit a good convergence property. This experimental result shows that the proposed method can find a compromise between regularity to remove noise and preserving image fidelity.

1. INTRODUCTION

Spatial image degradation in remotely sensed imagery happens in many ways. For remote sensing imaging, image acquisition occurs while orbiting the earth. During image acquisition, the imaging system causes a blurring due to the cumulative effects of the instrumental optics and image motion by satellites' orbit manoeuvring (Schott, 2007). This blurring effect can be modeled by the Point Spread Function (PSF) or by the Modulation Transfer Function (MTF) in the frequency domain. Blurred images inherently have less information than sharp images, which leads to difficulty when performing image analysis and scene interpretation. Therefore, the MTF degradation needs to compensate for spatial quality improvement. Satellite image restoration based on compensation of MTF dates to mid-1980s but was not commonly available as production processing option until about the year 2000 (Schowengerd, 2007). The restoration kernel is called MTF compensation or commonly referred to as MTFC. MTFC based on image filtering techniques is the most commonly adopted method by most of the optical satellites. Generally, this type of method involves two steps. First, The MTF is derived from the degraded image by measuring edge (Kohm, 2004; Roland, 2015), pulse (Helder et al. 2006; Kameche & Benmostefa, 2016), points (Helder et al. 2006) or relative target (Wang et al., 2014; Keller et al., 2017); second, based on the measured MTF, a filter-based method is applied for compensating the MTF to restore the degraded image. Among others, Wiener filter (Mu et al., 2013), constrained least square filter (Oh & Choi, 2014) and regularized Inverse filter (Li et al., 2013) are the popular choice because they are closed-form solutions that could be solved efficiently via Fourier Transform (FT). The goal of existing MTFC is to partially compensate for the system response by boosting the attenuated higher spatial frequencies (Schowengerd, 2007). This attempt enhances fine spatial detail but unfortunately, because of the heavy-tailed properties of MTF, it introduces noise and an unacceptable amount of aliasing. These effects compromise the image's Signal to Noise (SNR). Consequently, users must evaluate the relative importance of image sharpness versus noise to their applications in deciding whether MTFC processing is appropriate (Schott, 2007). MTFC is an image restoration problem; it is an objective process where its goal is to reconstruct the original image spectrum $F(v,\omega)$ from its degraded observed version $G(v,\omega)$ using a priori knowledge of the degradation phenomenon $H(v,\omega)$ and $N(v,\omega)$. The degradation model in the frequency domain can be described as

$$G(v,\omega) = H(v,\omega) \circ F(v,\omega) + N(v,\omega) \quad (1)$$

where v and ω are the spatial frequency coordinates, $N(v,\omega))$ denote the random noise spectrum and H denotes the optical transfer function, which amplitude spectrum is the MTF. The symbol $\circ$ denotes element-wise multiplication operator.

In practice, even if we could perfectly estimate the degradation function from a blurry image, restoring a coherent high frequency image details can still be very difficult. Because many different pairs $F(v,\omega)$ and $H(v,\omega)$, and/or $N(v,\omega)$ can give rise to the same $G(v,\omega)$, which make image restoration problem an ill-posed inverse problem. Thus, to create a well-posed problem, it is essential to incorporate prior information about the ideal image to constrain the restoration solutions. However, for an application like remote sensing, it is difficult to statically model the original image or obtain prior information about scenes never imaged before. Therefore, designing effective regularization terms to reflect the image priors for remotely sensed image restoration is at the core of this work.

There exists of a diverse variety of optimization approaches for regularized-based image inverse problem, particularly for natural images (i.e. consumer photograph, in the context of this work). In fact, a large class of pixel-based regularization terms that built on the well-known total variation (TV) (Rudin et al. 1992) demonstrate high effectiveness in preserving edges and recovering smooth regions. One representative work from the literature that uses TV energy model as MTFC for remote sensing image is Li et al (2017). TV regularizer utilizes local structural patterns with underlying assumption that images are locally smooth except at edges; therefore, they usually smear out image details and cannot deal well with fine structures. To take the advantage of the multi-scale property of images, sparsity-based regularization algorithms based on wavelet (Mallat, 1989), curvelet Candes & Donoho, 2000), and contourlet (Do & Vetterli, 2005) transforms are proposed. Sparsity-based regularizers force the transform domain coefficients of the restored images to be sparse, hence, they generally reduce noise without adversely affecting the restoration of edges. In most cases, the wavelet-type filters-based methods can achieved better quality than the TV-type based method. However, both regularization methods do not thoroughly make use of the all properties of the images. Recently, inspired by the success of nonlocal means (NLM) denoising filter by Buades et al. (2005) that exploits nonlocal self-similarity property of natural images, a series of patch-based regularization algorithms have emerged. Due to the utilization of self-similarity prior, this type of regularization terms has shown to produce superior results over the pixel-based regularizers, with sharper image edges and more image details (Zhang et al., 2014). However, it can be compromised with inaccurate sparse coding coefficients result, and often involves high computational as it is a large-scale non-convex optimization problem. The Pixel-based and patch-based regularizers are typically conducted in space domain. Convolution in the space domain incurs a high computational cost when compared with the cost of multiplication operation that is performed for the same filtering in the frequency domain. These two conditions are undesirable in any type of images, let alone remotely sensed image that is typically large and contains abundant texture with small details. On contrary, in frequency domain, owing to the fast Fourier transforms (FFTs), multiplications correspond to convolution operations can be accelerated which reduces computation burden, however, it still has its drawback. For example, the Wiener Filter. Wiener filter (Wiener, 1964) is the most widely used MTFC method, because it is simple, fast, and give good results in case of the relatively small blur. However, it is still an ill-posed problem although the MTF is known, so it gives rise to artifacts such as ringing and noise amplification in the restored image. Figure 1 illustrates some of the typical side effect of the restoration problem in spatial- and frequency-domain.

(a) (b) (c)

Figure. 1 Comparison of visual quality for image restoration in different domain. Red box denotes cropped region. (a) Original Image, (b) Restored image by Wiener filter (Mu et al., 2013), illustrating rise of ringing effect and noise amplification, and (c) Restored image by Anisotropic TV model (Pan et al., 2017), illustrating over smooth effect that created unnatural appearance.

Optical satellite image is typically large; packed with details in small scale. Hence, seeking a method that can find a compromise between regularity to remove noise and structure preservation, while retaining the spatial integrity in the restored image with minimum computation cost, is one of the most significant challenges in optical satellite image restoration problem. Based on the studies of previous work, two shortcomings have been discovered. First, only one image property used in regularization-based framework is not enough to obtain satisfying restoration results. Second, there is a need to design a framework for MTFC that exhibit the most appropriate compromise among computational complexity, reliability and robustness to noise. In this paper, we propose a framework for high-fidelity MTF compensation for optical satellite image restoration by characterizing both local smoothness and nonlocal self-similarity of images in minimum computational complexity. Given the fact that non-blind deconvolution can be regarded as separate step in the image restoration process, therefore, we consider the stand-alone problem, in other

words, a non- blind MTF Compensation, where given a blurry noisy input image, a known PSF, and a sharp image (i.e. original image) with shared content, how can we reliably remove blur and noise to restore coherent image details?

The remainder paper is organized as follows. In Section 2 we briefly describe some common characteristic from the perspective of image statistic and optimization approach that we employ to design our MTFC framework. Next, Section 3 introduces the objection functions containing regularization terms in the bilevel optimization problem and elaborate the details of solving optimization. The experimental results and discussions are provided in Section 4. Finally, Section 5 concludes this paper and points out possible directions for further research.

2. PROPOSED STRATEGIES AND SOLUTIONS FOR MTFC

In this section, we briefly describe the strategies and solutions that we apply to design an MTFC framework to attain the objectives of this work.

2.1. Image characteristics

Given a blur and noisy image, the goal of image restoration is to reliably remove blur and noise to restore coherent image details. The blurred-noisy image $g(x,y)$ corresponds to expression of Eq. (1) in the spatial domain is formulated as

$$g(x,y) = f(x,y) \oplus h(x,y) + \eta(x,y) \tag{2}$$

where $f(x,y), h(x,y)$ and $\eta(x,y)$ represent latent image, PSF and unknown noise respectively; the symbol $\otimes$ denotes two-dimensional (2D) convolution operator; x and y are the continuous variables in x and y plane, respectively. In recent years, nonlocal self-similarity characteristic revealed by natural images has possibly become the most significant nonlocal statistics in image processing. As explained in Sec. 1, there are series of nonlocal regularization term for inverse problem. While these methods have demonstrated successful results, they come at the price of additional complexity, often accompanied by higher computational cost, which is not favourable in our framework. In general, the regularization solution that copes with the ill-posed nature of image restoration can be described in the following minimization problem as

$$\min_f \frac{1}{2}\|f \oplus h - g\|_2^2 + \lambda P(f), \tag{3}$$

where $\frac{1}{2}\|f \oplus h - g\|_2^2$ is the L_2 data-fidelity term, $P(f)$ is called the regularization term denoting image prior and λ is the regularization parameter. Over the years, many studies suggest that priors based on natural image statistics can regularize deblurring problems to yield better results. Besides, studies also shown that the marginal distributions of image statistic have significantly heavier tails than a Laplacian, that well modeled by a hyper-Laplacian. The marginal statistics of images are usually modeled by general Gaussian distribution (GGD) (Levin et al., 2007), the simplified form of GGD is defined as $\rho_{GGD}(f) \propto e^{-\gamma|\nabla f|^p}$, where $\nabla f = (\partial_x f, \partial_y f)^T$ is the gradient of the image f, γ and v are the shape parameters. The distribution $\rho_{GGD}(f)$ is a Gaussian distribution function if $p = 2$, and a Laplacian distribution function if $p = 1$. If $0 < p < 1$, then $\rho_{GGD}(f)$ is named as hyper-Laplacian distribution. More discussion about the value p can be found in the paper by Krishnan & Fergus (2009). The authors have done an impressive work in proposing a fast deconvolution method using hyper-Laplacian priors. Based on their works and many others (Cheng et al., 2019; Chang & Wu, 2015), we notice that regularization term using a hyper-Laplacian prior can obtain a clear image with main structures and few artifacts. From the description of the local smoothness and nonlocal self-similarity characteristic in image statistic, it implies that image properties can be perceived in three components, which comprises of smooth, texture and structure as illustrated in Figure 2. Therefore, we utilize three image priors, namely, the hyper-Laplacian priors, gaussian and Laplacian prior term to regularize the optimization solution in the proposed MTFC Framework. In the proposed framework, the hyper-Laplacian priors is designed to constraint the solution in preserving the structure component of non-local self-similarity, whereas the Laplacian priors is for preserving the texture component of non-local self-similarity.

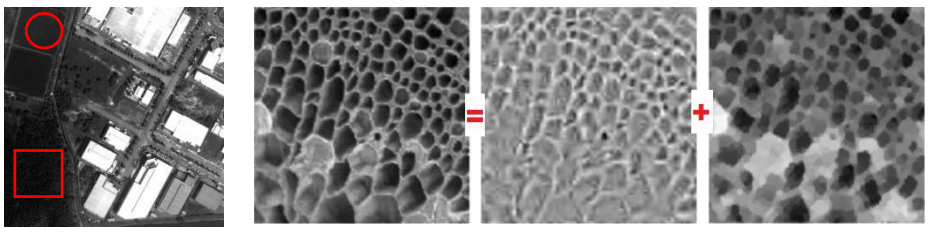

(a) (b) (c) (d)

Figure. 2 Illustration of image properties. (a) Satellite image contains example of local smoothness as shown by circular region, and nonlocal self-similarity as shown by square region, (b) a cropped region with nonlocal self-similarity properties, (c)-(d) depict decomposition of (b) into texture and structure region, respectively.

2.2. Hybrid Image Restoration Model through Bilevel Programming

Finding a compromise between regularity to remove noise and preserving image fidelity for natural images is unarguably a non-trivial problem. Hence, many approaches have been explored, which include hybrid approach. Some representative works in the literature are Joint Statistic Modelling (Zhang et al., 2014), Fourier-Wavelet Regularized Deconvolution (Neelamani et al., 2004), Hybrid TV-Hyper-Laplacian (Zhang et al., 2015) and Joint Non-Local Means Filter (Yang et al., 2014). These hybrid methods have demonstrated successful results. However, they require heavy mathematical model to carry out the task effectively, and consequently suffers from complexity of computation. Considering the respective advantages and limitations of different regularized-based approaches discussed in Sec.1, and the merit of different image prior characteristic in different image properties. In contrast to the methods in literature, we develop two regularization models with different objective function to characterize the image properties. We optimize the two-regularization model with multi-objective bilevel programming (MBP) for high fidelity of MTF compensation. To the best of our knowledge, image restoration techniques based on MBP has not yet received a broad attention in the literature. Only a few articles related to this class of problems in the literature (Tappen et al., 2007; Nikolova et al., 2015; Kunisch & Pock, 2013) were found, and the studies were mainly focusing at parameter learning for variational image denoising models. MBP has a few advantages as compared to the conventional iterative method that frequently use in image restoration technique, is that it can ease the difficulty of dealing with the disjunctive nature of the complementarity constraints and optimize many parameters simultaneously. In this study, we belief that MTF compensated image with significant improvement of signal to noise ratio can be achieved by incorporating the three image priors suggested in Sec. 2.1 into the ill-posed restoration problem. Solving it efficiently using the MBP is one of the main contributions of this work.

3. PROPOSED MODULATION TRANSFER FUNCTION COMPENSATION FRAMEWORK

In this framework, we develop two regularization model; one is used for characterizing the properties of image smoothness and image structure, whereas the other one is used for characterizing the properties of image texture. With these regularization terms, we fused the two complementary models in Curvelet domain to maximize their merits and minimize their weaknesses. In doing that, we can obtain a high-fidelity image that portray both local and nonlocal properties of image more richly, which confines the space of inverse problem solution and significantly improve the spatial quality of the observed image. The model for this framework is defined as

$$MTFC_3(F) = MTFC_1(F_A) + MTFC_2(F_{A`}), \text{ with } A' = \{s \in S: s \notin A\}. \quad (4)$$

where $MTFC_3(F)$, $MTFC_1(F_A)$, and $MTFC_2(F_{A`})$ represent the Hybrid MTFC Model, regularization model that contains image smooth and structure, and another regularization model that contains image texture. The $S = (s_0, \dots, s_{N_j})$ in which N_j is determined by

$$N_j = [log_2(\min(m, n) - 3], \quad (5)$$

where m and n are size of *F*. We decouple the two regularization terms in Eq. (6) into separate steps and optimize the solutions with multi-objective bilevel programming (MBP) such that they become lower level problem and upper level problem, respectively. In the next section, we first describe the Lower level problem and follow by Upper level Problem.

3.1. Lower Level Problem

The objective function for the lower level problem (LLP) is obtain a clear image that emphasize image smoothness without amplified noise and image structure without unwanted image artifacts such as ringing near edges. To achieve this objective function, we develop two strategies, where first we adopted a hyper-Laplacian image prior (Krishnan & Fergus, 2009) to make gradients in near-edge regions obey a heavy-tailed distribution to produce sharper edges; and to suppress noise and remove ringing artifacts. Secondly, we introduce a mask to encode edge regions and use a gaussian prior to eliminate noise and ringing artifacts in locally smooth regions. The combined image priors, is thus defined as

$$P(f) = \tau_1 \|\nabla f\|^p \circ M(x) + \tau_2 \|\nabla f\|_2^2 \circ (1_{\text{n x m}} - M(x)), \quad (6)$$

where $\nabla f = (\partial_x f, \partial_y f)^T$ is the gradient of the image *f*, τ_1, and τ_2 are the weights; the symbol $\circ$ represents the element-wise multiplication operator, $\|.\|^p$ is the hyper-Laplacian prior; *p* is the parameter with $\frac{1}{2} \leq p \leq \frac{4}{5}$ Smaller *p* leads to a smoother result. We can adjust *p* to get a satisfactory result. $1_{n \text{ x } m}$ denotes an all-ones matrix according to a *n* x *m* image, and *M*(*x*) is a 2D binary mask function. The proposed prior *P*(*f*) in Eq. (6) is used as a regularization term to solve the objective function of LLP. Hence, the total energy of LLP is defined as

$$MTFC_L(f_L) = \min_f \|f_L \oplus h - g\|_2^2 + P_L(\hat{f}_L) \quad (7)$$

$$\text{subject to } \hat{f}_L = argmin\ \tau_1\|\nabla f_L\|^p \circ M(x) + \tau_2\|\nabla f_L\|_2^2 \circ (1_{nxm} - M(x)),\ \tau_1 > 0,\ \tau_2 > 0$$

To solve the non-convex function of Eq. (7), we introduce an auxiliary variable u to substitute ∇f_L and add another regularization term to Eq. (7) to penalize non-sparsity of gradient. Therefore, Eq. (7) can be rewritten as

$$\begin{aligned} &MTFC_L(f_L) = \min_{f_L}\|f_L \oplus h - g\|_2^2 + P_L(f_L) \\ &\text{subject to } \hat{f}_L = \min_{f_l} \tau_1\|u\|^{p\circ}M(x) + \tau_2\|u\|_2^{2\circ}(1_{nxm} - M(x)) + \tau_3\|\nabla f_L - u\|_2^2,\ \tau_1 > 0,\ \tau_2 > 0. \end{aligned} \tag{8}$$

When τ_3 is close to ∞, the solution of Eq. (8) converges to that of Eq. (7). With the formulation of Eq. (8), we can decouple the optimization problem into two sub-problem and solve them efficiently through alternatively minimizing (Geman & Yang, 1995) *f* and *u* independently. Accordingly, we briefly describe the following two sub-problem for which we call u^L sub-problem and f^L sub-problem.

u^L sub-problem: By fixing all variables except u, Eq. (8) is reduced to

$$\tau_1\|u\|^{p\circ}M(x) + \tau_2\|u\|_2^{2\circ}(1_{nxm} - M(x)) + \tau_3\|\nabla f_L - u\|_2^2. \tag{9}$$

Thus, we can find optimal *u* using Newton-paphson method. The variables p, $\tau_1\tau_2$ and τ_3 are empirically set to 2/3, 0.001, 0.01 and 0.1, respectively.

f^L sub-problem: Given a fixed value of *u* from the previous iteration, Eq. (9) is quadratic in *f*. The optimal f_L is thus become

$$\min_{f_L}\|f_L h - g\|_2^2 + \tau_3\|f_L - u\|_2^2. \tag{10}$$

As it is a closed-form least squares minimization problem, this allows us to find optimal *f* directly using FFTs based on Parseval's theorem. To demonstrate the contribution of Eq. (10), we conduct an experiment as shown in Figure.3. From Figure 3, it can be observed visually that the proposed image priors provide structure preservation better than Krishnan & Fergus (2009). Another observation is that the boundary artifacts due to the periodicity property of FT are not visible in intermediate latent image f_L.

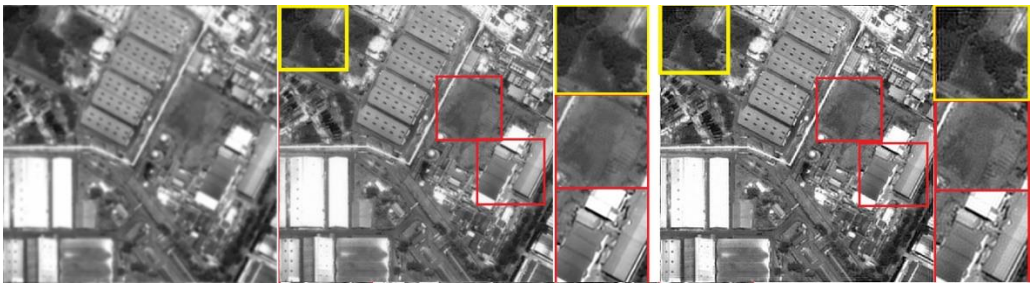

Figure. 3 Effectiveness of the proposed prior, the block regions show the cropped region and their closed-up view. (a) Blurred-noisy input (gaussian blur, $\boldsymbol{\sigma}$ **=2)**, (b) intermediate latent image f_L restored by Eq. (10). (c) Restored results using method by Krishnan & Fergus (2009). Closed-up view from the yellow box obviously shown boundary artifacts.

3.2. Upper Level Problem

The upper level problem (ULP) comprises two objective functions, one is to recover the fines texture of the degraded image spectrum *G* based on $\bar{f}_L \in X_L(f_U)$, while the other one is to produce the ultimate restoration result. Similar to LLP, we solve the ULP in two steps; the two steps problem is described as u^U sub-problems and f^U sub-problems.
u^U sub-problem: The objective function corresponds to solving the upper level problem (ULP) is defined as

$$MTFC_U(F_U) = \frac{\overline{H(v,\omega)}}{|H(v,\omega)|^2 + \alpha|R(v,\omega)|^2} \circ G(v,\omega), \text{ subject to } \|g - Hf_L\|^2 = \|\eta\|^2, \alpha > 0, \tag{11}$$

where *v* and *ω* are the spatial frequency coordinate; α is a weight, $R(v,\omega)$ is a Laplacian prior, which penalizes the PSFs that are not smooth; and $\overline{H(.)}$ is the complex conjugate of *H*. Note that Eq.(11) has the same expression as the constrained least squares (CLS) filter defined in Li et al.(2013). The regularization term Eq. (11) has the advantages of convex optimization and a very low computational complexity. There is no need to design a very complex regularization term, since the task of restoring smooth regions and retaining the sharp edges will be accomplished by LLP. Nevertheless, to make Eq. (11) more tractable and robust, we introduce another prior term about the solution as

$$P_U(f_U) = \varepsilon/Var(f_L), \tag{12}$$

where ε is the noise level estimation using the method by Liu et al. (2013) and $Var(f_L)$ is the image variance of the estimate undegraded image (i.e. the output from LLP). The main problem of the classic CLS filter in image restoration is that the weights could not be estimated accurately based on the blurred noisy image. If a reference image that contains a much better estimate of the frequency information than the noisy image is available, then the regularization term could be estimated more accurately. In addition, optimization of UPP is more efficient because α can be found

must faster than the classic one. With introduction of Eq. (12), the objection function and constraints of ULP in Eq. (11) are modified to become

$$MTFC_U(\bar{F}_U) = \frac{\overline{H(v,\omega)}}{|H(v,\omega)|^2 + \alpha P_U(f_L)|R(v,\omega)|^2} \circ G(v,\omega), \text{subject to } min\ \|f_L - f\|_2^2, \alpha > 0, \varepsilon - \|f_L - f\|_2^2 = 0, \quad (13)$$

where $min\ \|f_L - f\|_2^2$ denotes image fidelity of LLP. Figure 4 and 5 presents comparison of visual image quality and convergence analysis between the improved CLS and classic CLS, respectively. From the closed-up views in Figs 4(b) and 4(c), it can be noticed that the proposed CLS produce sharper results than the classic CLS. Whereas from Figure 5, It can be noted that the improved CLS converges much faster than the classical one, where it requires only 30 iterations as stop criterion, which is six times faster than the classic CLS.

(a) (b) (c)

Figure 4. Visual quality comparison of image restoration (a) Blurred-noisy input (gaussian blur, σ =2), (b) Restored results by the proposed improved CLS using Eq. (20), (c) Restored results by classic CLS. Note that the close-up views correspond to red box in (b) and (c).

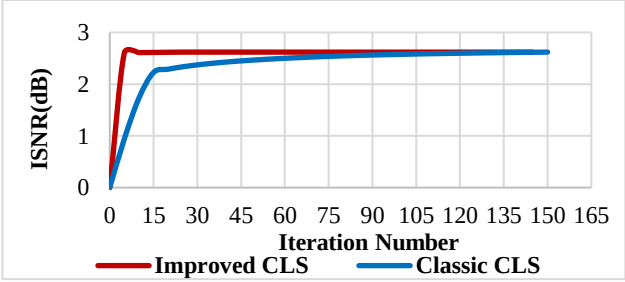

Figure 5. Convergence analysis for improved CLS and classic CLS

$\mathbf{f}^U$ sub-problem: The objective function corresponds to combine local and nonlocal properties of image from the bilevel problem, and implicitly determine the most optimal decision of this problem is defined as

$$MTFC_U(f_U, f_L) = C^{-1}\left[\langle \bar{f}_U, \psi^u_{j,p,k}\rangle + \langle \bar{f}_L, \psi^l_{j,p,k}\rangle\right], \text{subject to } Q(f_L), Q(f_U) > Q(\bar{f}_U) : \bar{f}_U \in X_U \quad (14)$$

where C^{-1}denotes the inverse curvelet transform function; $\psi^u_{j,p,k}$is the curvelet coefficient of Latent image from ULP at scale *j*, wedge location *p*, and coordinates *k*, whereas $\psi^l_{j',p,k}$ is the curvelet coefficient of Latent image from LLP at scale *j`*(i.e., complement of *j*). For all images in $f = (f_U, f_L)$ with the size of *m* x *n* pixel, we use Eq. (5) to calculate the number of scales and apply bandpass filtering to extract frequency coefficients of f at each scale and filter into pool of subbands as follow

$$\left\{f_U \mapsto (\Delta_0 f_U, \Delta_1 f_U, \Delta_2 f_U, \dots \Delta_{N_j} f_U), f_L \mapsto (S_0 f_L, \Delta_1 f_L, \Delta_2 f_L, \dots \Delta_{N_j} f_L)\right\}, \quad (15)$$

where $\Delta_{0\dots N_j}$ represent the band levels, with Δ_0 being the band with lowest frequencies, and Δ_{N_j} being the band with the highest frequencies. Since low frequencies responsible for general appearance of image over smooth areas, whereas high frequencies responsible for detail. As we select $f_L \mapsto (\Delta_0 f_L, \Delta_1 f_L, \Delta_{N_j} f_L)$ to represent the smoothness region and structure, then the texture will be presented by $f_U \mapsto (\Delta_2 f_U, \Delta_3 f_U, \dots, \Delta_{N_{j-1}} f_U)$. Thus, finally, we obtain the final decision of MBP as $f \mapsto (\Delta_0 f_L, \Delta_1 f_L, \Delta_2 f_U, \Delta_3 f_U, \dots, \Delta_{N_{j-1}} f_U, \Delta_{N_j} f_L)$, which is the ultimate restoration result.

4. ANALYSIS AND EXPERIMENTAL RESULTS

In this section, we present extensive experimental results to evaluate the performance of the proposed algorithm. The datasets that we used are synthetically blurred satellite images simulated from level 2A product of IKONOS, which is also the ground-truth data for this experiment. As the practical atmospheric PSF in remote sensing images is assumed to be a Gaussian-like shape, so we synthetically blurred the ground truth with Gaussian blur for six different

standard deviation (SD) σ of 1, 1.5, 2, 2.6, 3 and 4. Apart from blurring, we also added white additive Gaussian noise with zero mean and 0.5 SD to all synthetic data to test the robustness of the proposed algorithm. We compare our proposed algorithm with five competing methods. They comprise of an MTF-filtering based method which is the widely used Wiener filter, two recent representative non-blind deconvolution methods (i.e., Krishnan & Fergus (2009) and Pan et al. (2017)) that exploit image prior as regularization term, and two representative non-blind deconvolution methods (i.e., Zhang et al. (2014), Zhang et al. (2015)), which use hybrid model. We evaluate the competing methods from two aspects: effectiveness and efficiency. To evaluate effectiveness, we use ISNR (unit: dB), and the recently proposed FSIM [unitless: interval [0 1]); FSIM is known to achieve much higher consistency with the subjective evaluations than state-of-the-art image quality assessment metrics (Zhang et al., 2011). In addition to quantitative measurement, we also use visual observation for qualitative evaluation.

4.1. Analysis on the effectiveness of Combined Prior in MTFC

In this analysis, we collect four groups of 10 datasets with different blurring effects (i.e. σ of 1, 2, 3,4) to evaluate the effectiveness of the proposed combined prior in MTFC. For each restored image f by the proposed regularization-based MTFC method, we decompose it into subbands in curvelet domain and measure its FSIM with reference to ground truth. Table 1 tabulates the average FSIM and relative SD of each subband for all datasets. From the analyses, it is expected that the dataset with the smallest blurring effect will produce the best image reconstruction results with smallest uncertainty, vice versa. In addition, this analysis shows that the proposed combined prior can preserve structure effectively even in large blur condition. One key observation is that the proposed prior can attain near perfect FSIM score in the mid-range frequency, which indicates that it can preserve image detail effectively. Moreover, it can be noted that even with large gaussian blur $\boldsymbol{\sigma}$ **=4,** the proposed method is capable to recover the high frequency components of image up to 0.90352 FSIM value with relative SD as low as 0.006%. The low uncertainty values of the reconstructed subbands tabulated in Table 1 demonstrate high reliability of the priors employed by the proposed method. This merit can warrant the robustness of the proposed method.

Table 1 The average FSIM and relative SD of datasets in their respective subband.

Subband	**Dataset 1**		**Dataset 2**		**Dataset 3**		**Dataset 4**	
	σ **=1**		σ **=2**		σ **=3**		σ **=4**	
	Average FSIM	Relative SD (%)	Average FSIM	Relative SD (%)	Average FSIM	Relative SD (%)	Average FSIM	Relative SD (%)
$\Delta_0 f$	0.99999	0.0001	0.99967	0.0089	0.99999	0.0010	0.99864	0.0027
$\Delta_1 f$	0.99998	0.0039	0.99970	0.0065	0.99992	0.0084	0.99989	0.0030
$\Delta_2 f$	0.99996	0.0064	0.99029	0.0106	0.99943	0.9385	0.99189	0.0420
$\Delta_3 f$	0.99998	0.0039	0.99884	0.0091	0.99928	0.0095	0.97167	0.0052
$\Delta_4 f$	0.99921	0.0062	0.94080	0.0039	0.93902	0.0098	0.92584	0.0013
$\Delta_5 f$	0.99229	0.0031	0.92120	0.0055	0.92091	0.0145	0.90352	0.0061

Figure 6 presents examples of synthetic blurred-noisy images used in this analysis and their respective restoration results by the proposed regularization-based MTFC method. In Figure 6, quantitative measurements value at the left of the slash denotes ISNR (dB) and the right of the slash denotes FSIM.

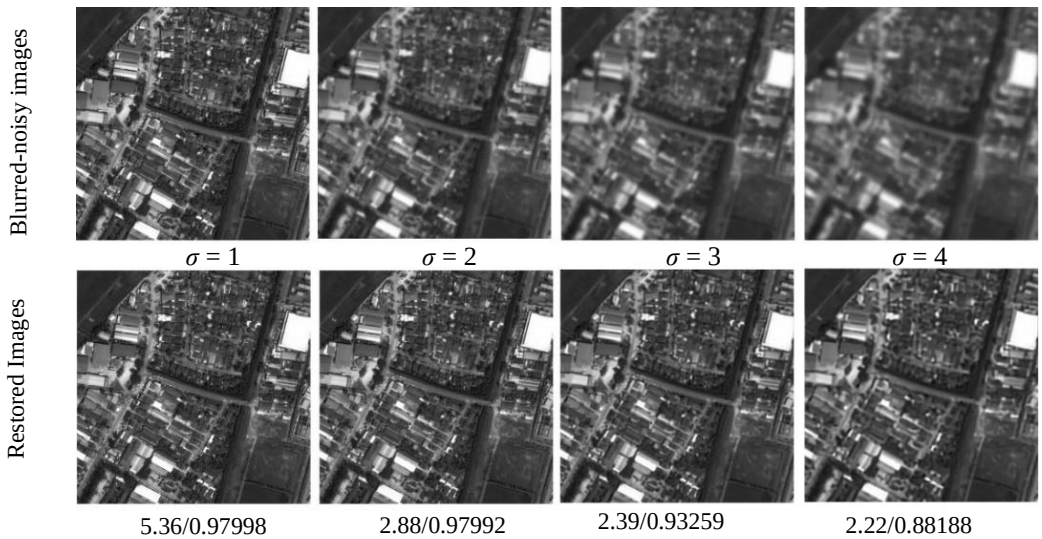

Figure 6. Restoration results; The top row shows blurred-noisy image with different amount of blur, whereas bottom row presents respective image after image restoration process.

4.2. Comparison with competing methods

In this sub-section, we present experimental evaluations for spatial quality improvement by the proposed regularization-based MTFC method against five competing methods. Table 2 tabulates some of the FSIM and ISNR results among competing methods on the datasets. These results are generated using the same input blurry images and PSF kernel, hence they are directly comparable. From Table 2, we have several observations. Firstly, the proposed method considerably outperforms the other methods in term of FSIM, with about 95% (i.e. 38 of 40 cases) the highest FSIM in all the cases. However, in term of ISNR, the proposed MTFC method is outperformed by Zhang et al. (2014), with the second highest ISNR in all cases. Secondly, we observed that in the case of $\sigma = 3$ and $\sigma = 4$ on image P3 (P3 is illustrate in second row of Figure 8(h) method by Zhang et al. (2014) that uses patch-based regularization method achieves better FSIM than the proposed method. This demonstrates that patch-based regularization method is more effective in preserving structure of images with less detail. Therefore, from this table, we conclude that the proposed MTFC method is comparable to the Hybrid methods, and significantly outperformed the widely used Wiener filter and image prior-based regularization methods, with better ISNR and FSIM results in all cases.

Table 2 FSIM and ISNR comparison of various regularization method for image restoration.

Gaussian blur, $\boldsymbol{\sigma}$ **=1**												
	MTF-based Filtering		Prior-based Regularization Method				Hybrid / Joint Statistical Regularization Method					
Data	Wiener Filter		(Krishnan & Fergus (2009)		(Pan et al. 2017)		(Zhang et al., 2015)		(Zhang et al., 2014)		Proposed Method	
	FSIM	ISNR	FSIM	ISNR	FSIM	ISNR	FSIM	ISNR	FSIM	ISNR	FSIM	ISNR
P1	0.99772	1.55	0.99751	3.57	0.99704	2.69	0.99652	4.31	0.99655	7.56	0.99856	6.96
P2	0.98172	0.62	0.97974	2.40	0.97891	2.02	0.97848	3.65	0.97850	5.49	0.97859	4.26
P3	0.98308	2.78	0.9814	2.92	0.97974	3.33	0.97941	4.89	0.97951	7.81	0.98153	5.84
P4	0.99516	0.52	0.99754	5.05	0.99621	2.22	0.99757	5.05	0.99764	6.84	0.99861	5.65
Gaussian blur, $\boldsymbol{\sigma}$ **=2**												
P1	0.97957	3.34	0.97936	2.66	0.97957	2.72	0.97855	2.65	0.97957	3.97	0.97961	3.57
P2	0.98043	1.86	0.97974	1.30	0.97891	1.48	0.97848	1.85	0.97850	2.26	0.97891	2.19
P3	0.98308	1.97	0.98140	1.32	0.97974	1.30	0.97941	1.72	0.97951	3.09	0.98051	2.90
P4	0.98062	2.25	0.98093	2.64	0.98005	1.77	0.98100	2.64	0.98100	3.09	0.98297	2.65
Gaussian blur, $\boldsymbol{\sigma}$ **=3**												
P1	0.93423	2.45	0.93382	2.34	0.93251	1.82	0.93415	2.44	0.93426	2.72	0.93430	2.46
P2	0.94192	1.85	0.92645	1.85	0.94043	1.40	0.94202	1.89	0.94339	2.01	0.94596	1.91
P3	0.92842	0.98	0.92841	0.84	0.92718	0.53	0.92828	0.80	0.92996	1.72	0.92952	1.60
P4	0.93539	2.39	0.93075	1.55	0.93372	1.64	0.92901	1.96	0.93554	2.77	0.93594	2.43
Gaussian blur, $\boldsymbol{\sigma}$ **=4**												
P1	0.88259	2.49	0.88287	2.48	0.86666	1.82	0.88330	2.32	0.88196	2.66	0.88227	2.51
P2	0.86651	1.88	0.86536	1.88	0.86267	1.40	0.86295	1.76	0.86651	2.01	0.86693	1.93
P3	0.86833	2.48	0.86823	2.42	0.86830	1.88	0.86840	2.48	0.87576	2.63	0.87409	2.54
P4	0.88088	2.38	0.88150	2.37	0.87471	1.55	0.88112	2.38	0.88020	2.66	0.88188	2.49

Figures 7 and 8 show visual quality restoration results for some of the data in Table 2. Only four examples are shown, and each represents restoration for a different amount of blur. Note that these examples are selected based on their feature density in a scene. In figures 7, quantitative measurements value at the left of the slash denotes ISNR (dB) and the right of the slash denotes FSIM. From visual observation, it is apparent that all the methods produce sharper image than the blurred-noisy image. From the closed-up view, we observe noise amplification in restored results by Wiener filter; The method by Krishnan and Fergus (2009) is good at capturing contour structures but fails in recovering textures and produces over-smooth effects. We observe that method (Krishnan and Fergus, 2009) can restore better texture than method (Pan et al., 2017), however it produces noticeable boundary artifacts. These artifacts can be overcome to some extend with edge tapering operations. Meanwhile, hybrid method by Zhang et al. (2015) can restore textures better than the method by Krishnan and Fergus (2009) and suppresses most of the noise-caused artifacts, however it is exhibiting a lower contrast visual quality than other methods. Among all, the hybrid method by Zhang et al. (2014) produces much cleaner image with sharper edges and textures, however for large blur image, it tends to produce unnatural appearance (i.e. cartoon effect) on restored image as shown in Figure 7. Based on this experiment, we found that the proposed regularization-based MTFC method can provides accurate restoration on both edges and textures with almost unnoticeable ringing artifacts. It is exhibiting good visual quality, which is consistent with FSIM. While it may not have producing visual quality as clean as method (Zhang et al., 2014), but it exhibits a more natural effect than other methods, including method (Zhang et al., 2014) for large blurred image.

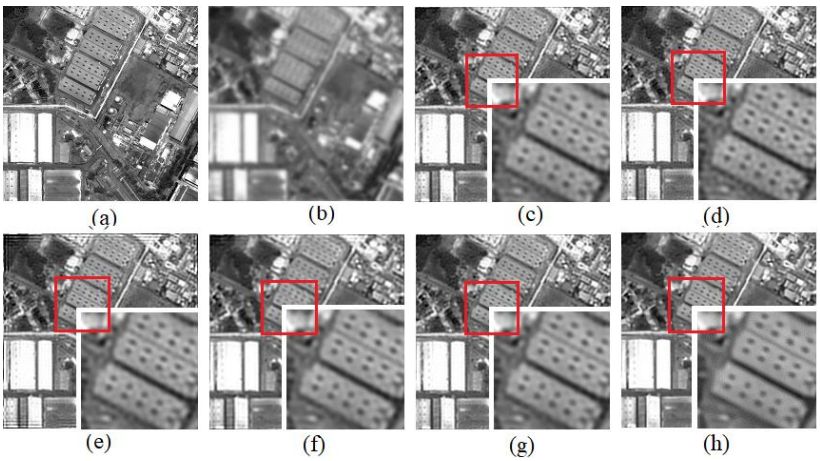

Figure 7.Visual quality comparison of image restoration in the case of blur $\boldsymbol{\sigma}$ **=4**, red box denotes cropped region (a) Original image, (b) Blurred-noisy image, P4 (c)-(h) restoration results by the proposed method (2.49dB/0.88188), Wiener filter (2.38dB/0.88088 Krishnan & Fergus (2009)(2.37dB/0.88150), Pan et al.(2017)(1.55dB/0.87471), Zhang et al.(2015) (0.80dB/0.92828), and Zhang et al.(2014)(2.66dB/0.88020).

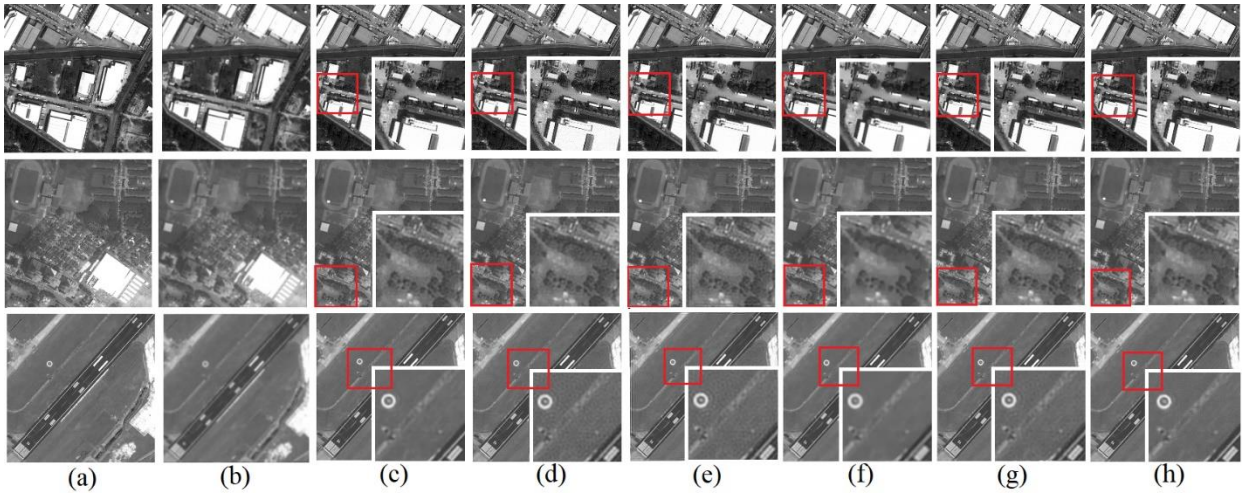

Figure 87. Visual quality comparison of image restoration for P1(first row), P2 (second row) and P3 (third row) in the case of blur $\boldsymbol{\sigma}$ **= 1,** $\boldsymbol{\sigma}$ **= 2, and** $\boldsymbol{\sigma}$ **=3**, respectively. Red box denotes cropped region (a) Original image, (b) Blurred-noisy image, P4 (c)-(h) restoration results by; (c) the proposed method, (d) Wiener filter, (e) Krishnan & Fergus (2009), (f) Pan et al.(2017), (g) Zhang et al.(2015), and (h) Zhang et al.(2014).

4.3. Algorithm Complexity and Computational Time

We implemented our method in MATLAB on an Intel Core i5 CPU with 8 GB of RAM. Comparing the u^L, u^U, f^L, f^U sub-problems in the bilevel programming, it is obvious to conclude that the main complexity of the proposed algorithm comes from the u^U sub-problem. However, as the primary computational task in both upper and lower level problem consists of FFT, therefore, overall it has a very low computational complexity. In our implementation, for image of size 512×512, the bilevel optimization costs (9.47 ± 0.31) seconds. We present the computational time of all competing methods on the test images in Table 1. Form the table, it is obvious that Wiener Filter is the fastest method. Method by Krishnan and Fergus (2009) and Pan et al. (2017) come in second and third fastest, respectively. The proposed method being the fourth fastest. Although Zhang et al. (2014) has highest ISNR in most case, it suffers from huge computational times due the need for dictionary learning. It is about 120 times slower than the proposed method. From the table, unlike method by Krishnan & Fergus (2009), Pan et al. (2017), Zhang et al. (2015), and Zhang et al. (2014), the computational complexity of the proposed method and Wiener filter are independent of the amount of blur.

Table 3 Average run time (seconds) of different methods on images of size 512×512.

Gaussian blur, σ	Wiener Filter	(Krishnan & Fergus (2009)	(Pan et al. 2017)	(Zhang et al., 2015)	(Zhang et al., 2014)	Proposed Method
1	0.15	0.69	4.80	9.89	1016.15	9.34
2	0.18	0.79	4.38	10.79	1065.73	9.35
3	0.21	1.06	4.79	11.78	1103.34	9.89
4	0.24	1.25	4.29	12.64	1254.18	9.56

5. CONCLUSION

This paper describes a robust and efficient MTF compensation method for restoring optical satellite images with high fidelity using joint statistical model in Curvelet domain. In this work, we exploited the merit of image prior characteristic in the local smooth and nonlocal self-similarity properties of an image, to design an effective regularization term to solve the underdetermined inverse problem of MTFC. In particular, we show that the regularization-based MTFC can be reformulated as a tractable optimization problem using the MBP. To evaluate the performance of the proposed method, we performed extensive comparisons against leading methods in non-blind deconvolution, which included image quality assessment using ISNR, FSIM and computation time. The evaluation results show that the proposed method achieves significant performance in preserving more image details and exhibit good convergence property with minimum computational complexity. This indicates the proposed regularization-based MTFC method found a compromise between solution accuracy and computational efficiency, which is can be used to compensate the degradation for image spatial quality improvement. The successful results of patch-based regularization that exploits the nonlocal self-similarity properties of image in preserving high fidelity image is inarguable. However, it compromises with high computational complexity. Therefore, for future work, we would like to study the feasibility of this regularization term in MTFC and explore ways to improve its efficiency.

REFERENCES

Buades, A., Coll, B., and J. M. Morel, 2005. A non-local algorithm for image denoising. Int. Conf. on Computer Vision and Pattern Recognition, pp.60–65.

Candès, E. J. and Donoho, D. L., 2000. Curvelets, multiresolution representation, and scaling laws. Wavelet Applications in Signal and Image Processing VIII, SPIE Vol., 4119, pp.1–12.

Chang, C. and Wu, J., 2015. A New Hyper-Laplacian Prior-Based Deconvolution Method for Single Image Deblurring. 4(1), pp.9–18.

Do, M. N. and Vetterli, M., 2005. The contourlet transform: An efficient directional multiresolution image representation. IEEE Trans. Image Process., 14(12), pp.2091–2106.

Geman, D. and Yang, C. 1995. Nonlinear image recovery with half-quadratic regularization. PAMI, 4, pp.932– 946.

Helder, D., Choi, J., and Anderson, C., 2006. On-orbit modulation transfer function (MTF) measurements for IKONOS and QuickBird. In Proc. of the JACIE 2006 Civil Commercial Imagery Evaluation Workshop, Brookings, USA, pp.14–16.

Kameche, K., and Benmostefa, S., 2016. In-flight MTF stability assessment of ALSAT-2A satellite. Adv. Sp. Res., 58(1), pp.117–130.

Keller, G., Chang, T., and Xiong, X., 2017. MTF analysis using lunar observations for Himawari-8/AHI. In Proc. SPIE. 10402: Earth Observing Systems XXII.

Kohm, K., 2004. Modulation transfer function measurement method and results for the orbview-3 high resolution imaging satellite. in 20th Int. Cong. Photogrammetry and Remote Sensing, Int. Archives Photogrammetry.

Krishnan, D. and Fergus, R., 2009. Fast image deconvolution using hyper-Laplacian priors. in Proc. of in Advances in Neural Information Processing Systems. 22, pp.1–9.

Kunisch, K. and T. Pock, T., 2013. Bilevel Optimization Approach for Parameter Learning in Variational Models. SIAM Journal on Imaging Sciences, 6(2). pp.938–983.

Levin, A., Fergus, R., Durand, F., and Freeman, W., 2007. Image and depth from a conventional camera with a coded aperture. In Proc. SIGGRAPH: ACMTOG, 26(3), 70.

Li, J., Liu, Z., and Liu. F., 2017. Using sub-resolution features for self-compensation of the modulation transfer function in remote sensing," Optics Express, 25(4), 4018.

Li, X. Gu, X., Fu, Q., Yu, T., Gao, H., Li, J. and Liu, L., 2013. Removing atmospheric MTF and establishing an MTF compensation filter for the HJ-1A CCD camera. Int. J. Remote Sens. 34(4), pp.1413–1427.

Liu, X., Tanaka, M, and Okutomi, M., 2013. Single-image noise level estimation for blind denoising. IEEE Transactions on Image Processing, 22(12), pp.5226–5237.

Cheng, M. H., Huang, T. Z., Zhao, X., Ma, T. H., and Huang, J. A., 2019. A variational model with hybrid Hyper-Laplacian priors for Retinex," Applied Mathematical Modelling, 66, 305–321.

Mallat, S. G., 1989. A theory for multiresolution signal decomposition: the wavelet representation. IEEE Transactions on Pattern Analysis and Machine Intelligence, 11(7), pp674–693.

Mu, X., Xu, S., Li, G., and Hu, J., 2013. Remote sensing image restoration with modulation transfer function compensation technology in-orbit. In Proc. SPIE 8768.

Neelamani, R., Choi, H., and Baraniuk, R., 2004. ForWaRD: Fourier-Wavelet Regularized Deconvolution for Ill-Conditioned Systems. IEEE Transactions on Signal Processing, 52(2), pp.418–433.

Nikolova, M., Steidl, G., and Weiss, P., 2015. Bilevel Image Denoising using Gaussianity Tests. in: Scale Space and Variational Methods in Comp. Vision. Lecture Notes in Computer Science, 9087, Springer Int. Pub. pp.117–128.

Oh E. and Choi, J. K., 2014. GOCI image enhancement using an MTF compensation technique for coastal water applications. Opt. Express 22(22), pp.26908–26918.

Pan, J., Hu, Z., Su, Z., and Yang, M. H., 2017. L0-Regularized Intensity and Gradient Prior for Deblurring Text Images and beyond. IEEE Transactions on Pattern Analysis and Machine Intelligence, 39(2), pp.342–355.

Roland, J. K. M., 2015. A study of slanted-edge MTF stability and repeatability. in Proc. SPIE 9396: Image Quality and System Performance XII.

Rudin, L. I., Osher, S., and Fatemi, E., 1992. Nonlinear total variation-based noise removal algorithms," Phys. D., 60, pp.259–268.

Schott, J. R., 2007. Remote Sensing: The Image Chain Approach. 2nd edn., Oxford University Press, New York.

Schowengerdt, R. A., 2007. Remote Sensing: Models and Methods for Image Processing. 3rd ed. Academic Press.

Tappen, M. F., Liu, C., Adelson, E. H. and Freeman, W. T., 2007. Learning Gaussian Conditional Random Fields for Low-Level Vision. in Proc. of the IEEE Conference on Computer Vision and Pattern Recognition (CVPR), pp.1-8.

Wang et al., 2014. On-orbit characterization of MODIS modulation transfer function using the Moon. IEEE Trans. Geosci. Remote Sens., 52(7), pp.4112–4121.

Wiener, N., 1964. Extrapolation, Interpolation, and Smoothing of Stationary Time Series, MIT Press.

Zhang, L., Zhang, L., Mou, X., and Zhang, D., 2011. FSIM: A feature similarity index for image quality assessment. IEEE Trans. Image Processing, 20, pp.2378-2386.

Zhang, X., Wang, R. Tian, Y., and Wang, W., 2015. Image deblurring using robust sparsity priors. in Proc. IEEE International Conference on Image Processing (ICIP) pp.138–142.